Protection of HVDC Transmission Systems for Integrating Renewable Energy Resources

Mohamed S. Zaky
Electrical Engineering Department, College of Engineering, Northern Border University, Saudi Arabia
mohamed.zaky@nbu.edu.sa (corresponding author)

Hossam E. Ahmed
Electrical Engineering Department, College of Engineering, Northern Border University, Saudi Arabia | Electrical Engineering Department, Benha Faculty of Engineering, Benha University, Egypt
hossam.ahmed@nbu.edu.sa

Mahmoud Elsadd
Electrical Engineering Department, College of Engineering, Damanhour University, Egypt
mahmoud.elsadd@dmu.edu.eg

Mahmoud Elgamasy
Electrical Engineering Department, Faculty of Engineering, Menoufia University, Egypt
mahmoud.elgamasy@sh-eng.menofia.edu.eg

Received: 2 October 2023 | Revised: 19 October 2023 | Accepted: 24 October 2023

 DOI: https://doi.org/10.48084/etasr.6463

ABSTRACT

This paper introduces a fault locator approach designed for non-homogeneous VSC-HVDC (Voltage Source Converter-High Voltage Direct Current) transmission circuits. In various projects, such as those involving offshore wind farms, the transmission circuit's right-of-way can be non-homogeneous, incorporating a mix of underground cables and overhead lines. This diversity in circuit configuration poses issues with fault location approaches. The proposed method involves measuring signals at two sides of the non-homogeneous transmission circuit. Initially, the faulted section is identified using a specific criterion. This criterion calculates the profile of the 1-mode component of the voltage along the transmission circuit, without considering its non-homogeneous nature. This method is founded upon disparities in the voltage change rate between power cables and overhead lines. The provided identification method does not depend on the calculation of fault distances. Subsequently, the faulty point within the selected section is obtained by updating the calculated voltage profile. Notably, our method does not necessitate the installation of additional sensors at junction points. Furthermore, the introduced approach has the capability to locate various fault types, including pole-to-pole and pole-to-ground faults, and it remains effective regardless of the fault resistance value. These investigations were conducted using PSCAD software as a simulation environment, with the proposed method's calculations executed in MATLAB.

Keywords-fault location; VSC; HVDC transmission circuit;. offshore wind farm

I. INTRODUCTION

Voltage Source Converter-based High Voltage Direct Current (VSC-HVDC) transmission systems are widely employed worldwide for the efficient transmission of large power quantities. HVDC systems offer numerous advantages compared to traditional HVAC transmission systems [1-10]. One notable advantage is that the length of the DC transmission circuit is not limited, thanks to the absence of charging currents, especially with underground cables. This flexibility encourages the implementation of integration projects between different grids with varying frequencies over long distances. In some cases, the transmission system can be non-homogeneous, incorporating a mix of underground cables and overhead lines. This non-homogeneity arises due to the changing nature of the right-of-way, as seen in projects like offshore wind farms [11-15].

Accurately locating faults in HVDC systems is crucial for efficient maintenance, ensuring service continuity, and minimizing maintenance time [16-35]. One prominent approach in fault location methods is the traveling wave technique, which involves precisely determining when traveling waves from a faulty point arrive at the line ends by

analyzing time differences and wave speeds [16–26]. However, the accuracy of this method can be compromised when dealing with non-homogeneous transmission systems, where multiple specific values of wave speed may be present. Distinguishing among Reverberated waves originating from the fault location and other reflections, especially in non-homogeneous circuits, poses a challenge. The method presented in [27] addresses fault location in non-homogeneous circuits using the traveling wave concept, but it requires the installation of distributed current sensors at multiple points, including ends and junctions between overhead lines and underground cables. Other traveling wave methods employ specialized control arrangements, such as injecting traveling wave pulses through existing equipment like converters or hybrid DC circuit breakers [23, 24]. Some methods in this category involve on-site visits and the use of additional equipment, including waveform injectors, tracing monitors, and dedicated processing units [25, 26]. However, the presence of non-homogeneity in the transmission circuit can pose challenges for these methods.

Another category of fault location methods involves Machine Learning (ML) techniques [28-31]. These methods often rely on a large dataset composed of simulated or recorded test cases. The fault locator method in [28] utilizes the Pearson correlation coefficient to compare the measured voltage signals at the transmission system terminus against pre-existing manners. A similar approach is presented in [29], where the method checks the similarity of currents in the adopted DC breakers. To determine the fault location, a processing technique that involves weighted averaging with an approach based on kernel is employed. In [30], another fault locator method relies on neural networks and requires the high sampling rate of 5 MHz to capture traveling surges in currents. It is important to note that the non-homogeneity of the transmission system can add complexity when handling the required data for training in these methods.

Another category of fault locators is based on time domain calculations. Some methods utilize the Bergeron model representation for fault location [32-34]. This approach involves calculating the voltage profile along the length of the transmission system utilizing locally recorded voltage and current signals at the two ends. In a similar vein, the method described in [35] relies on time domain calculations with an estimated model for the transmission circuit. It is important to note that these models and time domain equations will not be suitable for non-homogeneous transmission systems. Additionally, an effective fault locator should be capable of locating all categories of faults, encompassing both pole-to-pole and pole-to-ground faults. Some methods in the literature are limited to locating ground faults only, relying on zero-mode components [21, 22]. The work in [31] is constrained to specific types of VSC converters.

The main contribution of this paper revolves around a fault localization technique that addresses the non-homogeneity of VSC-HVDC transmission circuits. The fault locator technique is based on a novel approach for identifying faulted sections, which hinges on variations in voltage rate changes between power cables and overhead lines. This identification method is not contingent on the computation of fault distances. Notably, it obviates the necessity of installing extra sensors at the junction points between underground cables and overhead lines. This method offers accurate fault location capabilities for all fault types, including pole-to-ground and pole-to-pole faults, without the complexity of calculations or the requirement for exceptionally high sampling frequencies.

II. THE PROPOSED FAULT LOCATION METHOD

Figure 1 illustrates the diagram of a non-homogeneous VSC-HVDC transmission line (two-section circuit): the underground cable section on the left portion and the overhead line section on the right portion. The proposed method consists of two steps. First, the fault section is determined, which could be either the underground cable section or the overhead section. Second, the method accurately identifies the fault's exact location within the previously selected section.

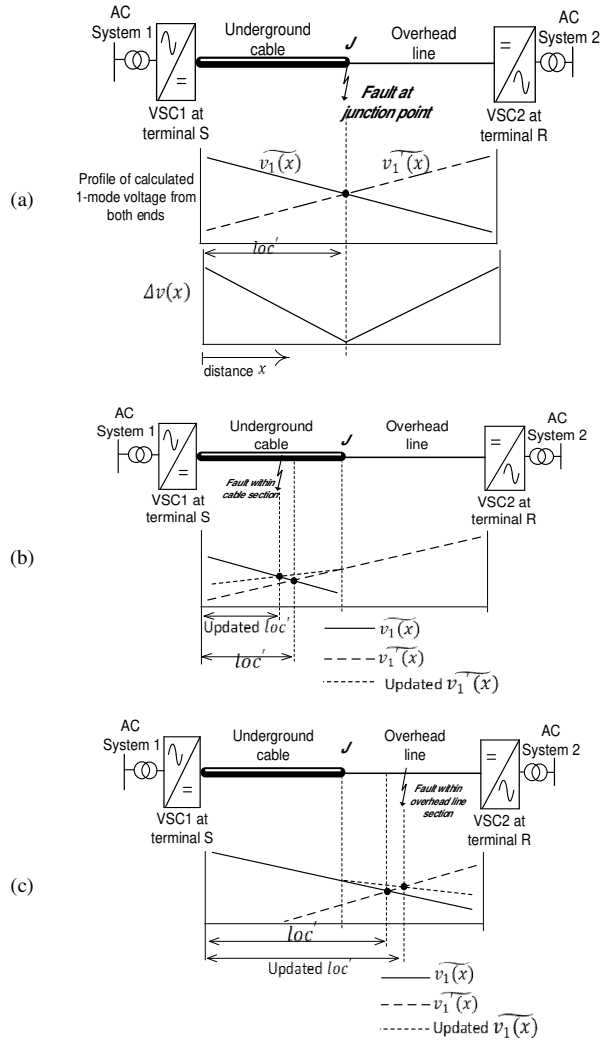

Fig. 1. The 1-mode voltage profiles calculated under different fault cases: (a) the fault is at the tie point among the underground cable and the overhead section, (b) the fault is within the underground cable section, (c) the faulty point is within the overhead section.

A. Fault Section Identification

The proposed method involves calculating the profile of the 1-mode voltage along the entire transmission circuit with reference to each terminal. The 1-mode voltage is determined at any distance *x* with respect to terminal *S* or terminal *R* using (1) and (2), respectively.

$$v_1(x,t) = \frac{1}{2}\left(\frac{z_{c1}+\frac{r_1 x}{4}}{z_{c1}}\right)^2 \left(v_{1S}(t+\tau 1) - i_{1S}(t+\tau 1)\left(z_{c1}+\frac{r_1 x}{4}\right)\right) + \frac{1}{2}\left(\frac{z_{c1}+\frac{r_1 x}{4}}{z_{c1}}\right)^2 \left(v_{1S}(t-\tau 1) - i_{1S}(t-\tau 1)\left(z_{c1}-\frac{r_1 x}{4}\right)\right) - \left(\frac{\frac{r_1 x}{4}}{z_{c1}}\right)^2 v_{1S}(t) - \frac{r_1 x}{4}\left(\frac{z_{c1}+\frac{r_1 x}{4}}{z_{c1}}\right)\left(\frac{z_{c1}-\frac{r_1 x}{4}}{z_{c1}}\right) i_{1S}(t) \quad (1)$$

$$v_1'(x,t) = \frac{1}{2}\left(\frac{z_{c1}'+\frac{r_1' x}{4}}{z_{c1}'}\right)^2 \left(v_{1R}(t+\tau 1') - i_{1R}(t+\tau 1')(z_{c1}' + \frac{r_1' x}{4})\right) + \frac{1}{2}\left(\frac{z_{c1}'+\frac{r_1' x}{4}}{z_{c1}'}\right)^2 \left(\begin{matrix} v_{1R}(t-\tau 1') - i_{1R}(t-\tau 1') \\ (z_{c1}' - \frac{r_1' x}{4}) \end{matrix}\right) - \left(\frac{\frac{r_1' x}{4}}{z_{c1}'}\right)^2 v_{1R}(t) - \frac{r_1' x}{4}\left(\frac{z_{c1}'+\frac{r_1' x}{4}}{z_{c1}'}\right)\left(\frac{z_{c1}'-\frac{r_1' x}{4}}{z_{c1}'}\right) i_{1R}(t) \quad (2)$$

where $v_1(x,t)$ and $v_1'(x,t)$ represent the 1-mode voltage components calculated at distance x with reference to terminals S and R, respectively. v_{1S}, i_{1S}, v_{1R}, and i_{1R} denote the 1-mode components of the measured electrical voltage and current readings at terminals S and R, respectively. These signals are calculated as functions of the measured positive and negative signals as follows:

$$v_1 = \frac{1}{\sqrt{2}}(v_p - v_n)\,,\; i_1 = \frac{1}{\sqrt{2}}(i_p - i_n) \quad (3)$$

where v_1, i_1 are the 1-mode voltage and current signals, while v_p, i_p, v_n, and i_n are the positive and negative voltage and current signals, respectively.

The parameters z_{c1} and r_1 stand for the 1-mode characteristic impedance and resistance per unit length of the underground cable, z_{c1}' and r_1' represent the corresponding values for the overhead line, and $\tau 1$ and $\tau 1'$ signify the 1-mode travel time duration along the underground cable and overhead line, respectively. The 1-mode parameters of the transmission circuit are calculated as follows:

$$r_1 = r_s - r_m\,,\; l_1 = l_s - l_m, c_1 = c_0 + 2c_m \quad (4)$$

where r_1, l_1, and c_1 are the 1-mode resistance, inductance, and capacitance of the transmission circuit, r_s, l_s, r_m, and l_m are the self and mutual parameters, and c_0 and c_m are the earth capacitance and the capacitance between poles, respectively.

It is worth noting that these profiles are calculated without considering the non-homogeneity of the transmission circuit. Based on (1) and (2), the profile of the 1-mode voltage along the transmission circuit is calculated as follows:

$$\widetilde{v_1}(x) = \frac{\sum_{t_1}^{t_2} v_1(x,t)}{(t_2-t_1)/\Delta t},\; \widetilde{v_1}'(x) = \frac{\sum_{t_1}^{t_2} v_1'(x,t)}{(t_2-t_1)/\Delta t} \quad (5)$$

$$\Delta v(x) = \left|\widetilde{v_1}(x) - \widetilde{v_1}'(x)\right| \quad (6)$$

$$loc' = x \text{ at the minimum of } \{\Delta v(x)\} \quad (7)$$

where $\widetilde{v_1}(x)$, $\widetilde{v_1}'(x)$ represent the normalized values of the 1-mode voltages at a particular point x throughout the post-fault period from t_1 to t_2, where t_1 marks the moment when the 1-mode voltage at the terminal point of the line decreases to a level lower than 0.9 per unit. Δt stands for the sampling time step, while Δv represents the difference between the calculated voltage profiles. loc' represents the initially determined fault location. It corresponds to the location at which $\Delta v(x)$ is minimized, as indicated in (7).

The identification of the faulted section is based on the initially determined value of loc'. If loc' is equal to the cable's longitudinal extent, it indicates that the fault is at the tie point among the cable and the overhead line. On the other hand, if loc' is less than the cable's length, it indicates that the fault lies within the segment of the underground cable. Alternatively, if loc' is greater than the cable's length, it confirms that the fault is in the overhead line segment.

For further clarity, the profiles of the voltage components corresponding to the 1-mode are illustrated under three fault scenarios in Figure 1. In Figure 1(a), when the fault takes place at the intersection point '*J*', the intersection point between the calculated 1-mode voltage profiles corresponds to the junction point, where $\Delta v(x)$ is minimized. In such a case, loc' equals to the cable's length. In other cases, when the fault is within the cable segment, loc' is less than the cable's length, as illustrated in Figure 1(b). If the fault is within the overhead line section, loc' is greater than the length of the cable, as illustrated in Figure 1(c). Figure 2 outlines the steps of the introduced approach for identifying the faulted section and locating the faulty point.

B. Determining Fault Location

After identifying which section is faulty, whether it is the cable or the overhead line segment, the fault location is determined. It is important to note that the initially determined value of loc' does not directly correspond to the fault distance, due to the non-homogeneity of the transmission system. Therefore, the profile of the 1-mode voltage needs to be updated beyond the junction point. As depicted in Figure 1, if the fault is within the underground cable segment, the profile of the 1-mode voltage must be updated along the cable segment utilizing the voltage and current signals at the junction point. Under such conditions, the overhead line section remains healthy. Thus, the voltage and current signals at the junction point can be straightforwardly computed based on the measured signals at the overhead end. Figure 1(b) illustrates how the 1-mode voltage profile is updated from the junction point towards the cable section. The fault distance is then estimated based on the intersection with the updated profile along the cable section.

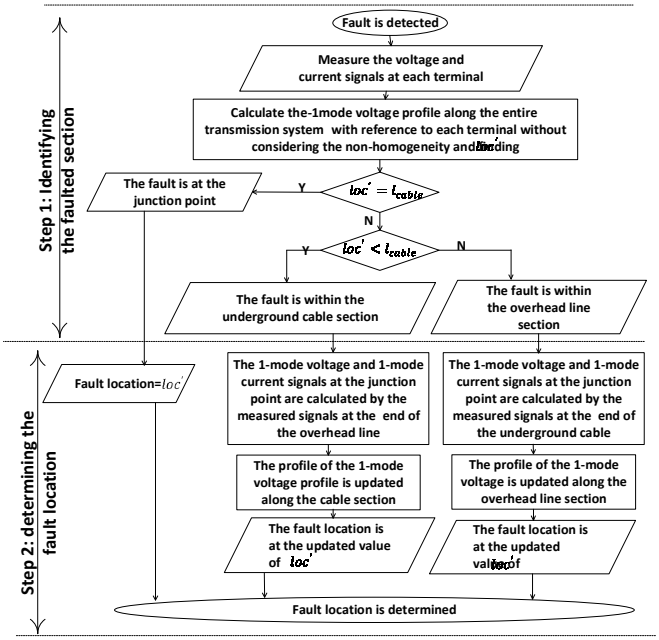

Fig. 2. The introduced fault location approach.

Similarly, if the fault is within the overhead line segment, as illustrated in Figure 1(c), the profile of the 1-mode voltage needs to be updated along the overhead line section using the voltage and current signals at the junction point. Under these conditions, the cable section is considered healthy. Thus, the voltage and current signals at the junction point are directly estimated utilizing the measured signals at the cable end. Figure 1(c) illustrates how the 1-mode voltage profile is updated from the junction point towards the overhead line section. The fault distance is then obtained based on the intersection with the updated profile along the overhead segment. To obtain the updated profile of the 1-mode voltage component along any of the sections, it is necessary to calculate the voltage and current signals at the junction point. The voltage at the junction point is calculated in the same manner as in (1) or (2). The current at the junction point is calculated by (8).

$$i_1(x,t) = \frac{1}{2z_{c1}}\left(\frac{z_{c1}+\frac{r_1 x}{4}}{z_{c1}}\right)\left(v_{1S}(t+\tau 1) - i_{1S}(t+\tau 1)\left(z_{c1} + \frac{r_1 x}{4}\right)\right) - \frac{1}{2z_{c1}}\left(\frac{z_{c1}-\frac{r_1 x}{4}}{z_{c1}}\right)\left(v_{1S}(t-\tau 1) - i_{1S}(t-\tau 1)\left(z_{c1} - \frac{r_1 x}{4}\right)\right) - \frac{1}{2z_{c1}}\left(\frac{r_1 x}{2z_{c1}}\right)\left(v_{1S}(t) - \frac{r_1 x}{4} i_{1S}(t)\right) \quad (8)$$

It is important to note that data windows of the measured signals need to be stored to perform the proposed calculations. In Figure 3(a), we can see the data windows of the recorded voltage and current readings at the ends of the transmission circuit. Figure 3(b) illustrates the necessary size of the data windows required for performing the proposed calculations.

As shown, to obtain the voltage profile calculated during the postfault duration from t_1 to t_2, the required size of the data window to be stored is $t_2 - t_1 + 4\tau$. This process is performed for each distance along the transmission circuit.

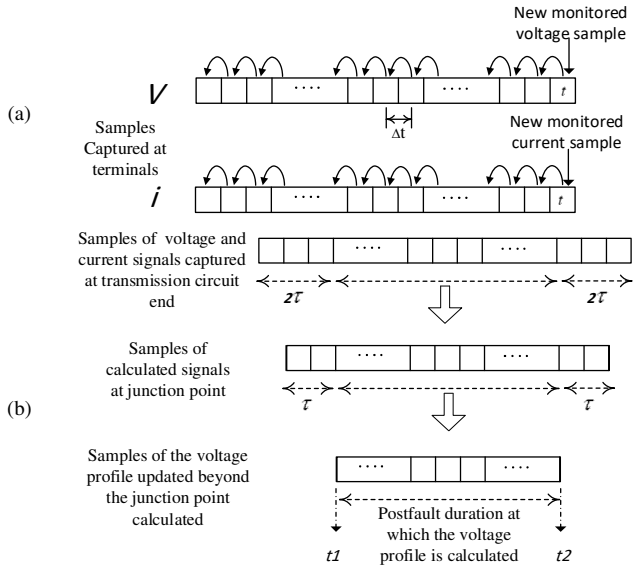

Fig. 3. Samples of the recorded voltage and current readings: (a) the data windows of the measured signals, (b) the required window size of the recorded readings and the corresponding window of the calculated samples of the voltage profile during post fault.

III. TEST SYSTEM DETAILS

Figure 4(a) displays a diagram depicting the simulated system with a single line used to validate the introduced fault-locator approach. This system stands as an illustration of the integration of an offshore wind farm with the grid via a non-homogeneous HVDC link. The simulated wind farm is a 450 MW DFIG (Doubly-Fed Induction Generator) type. The converters are simulated using their average dynamic models with the assistance of the PSCAD program. A non-homogeneous VSC-HVDC ±320 kV transmission circuit is simulated, and the underground cable and the overhead line configurations are presented in Figure 4(b). Details of the simulated MMC (Modular Multilevel Converter) units can be found in Table I. The HVDC voltage level is controlled by the converter on the onshore grid side, while the other converter on the offshore side is responsible for controlling the AC offshore voltage at the wind farm. Referring to the transmission circuit in Figure 4(a), each section, including the underground cable and the overhead line, has a length of 200 km. Various fault cases are simulated at different points, including the tie point among the underground cable and the overhead segments, within the cable section, and within the overhead line section, to investigate the proposed fault location approach. The sampling frequency utilized for capturing the measured signals is 50 kHz.

TABLE I. MMC PARAMETERS [11]

Parameter	value
The count of equivalent sub-modules per arm	76
Sub-module capacitance (μF)	3000
Arm inductance (mH)	50
Resistance due to capacitor leakage (MΩ)	10
Power (MW)	450
DC Voltage (kV)	±320

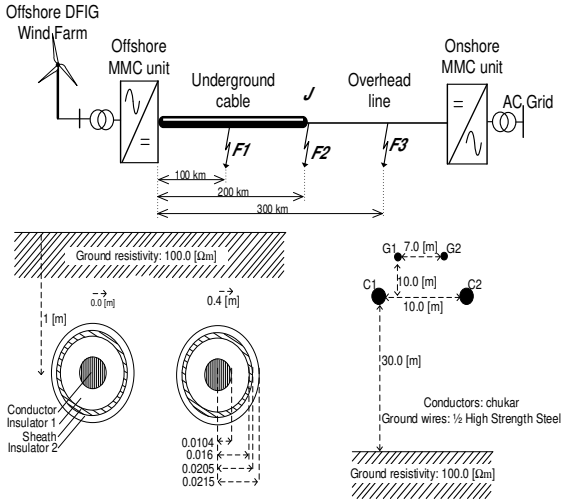

Fig. 4. (a) The simulated VSC-HVDC transmission circuit for integrating offshore wind farm to the grid, (b) the configuration of the underground cable and overhead line.

IV. VALIDATION RESULTS

A. Fault at the Junction Point

To investigate the introduced location approach, a pole-to-pole fault is simulated at *F2* at the junction point, which is 200 km away from both ends of the transmission circuit. The calculated profile of the 1-mode voltages along the entire transmission line is illustrated in Figure 5(a).

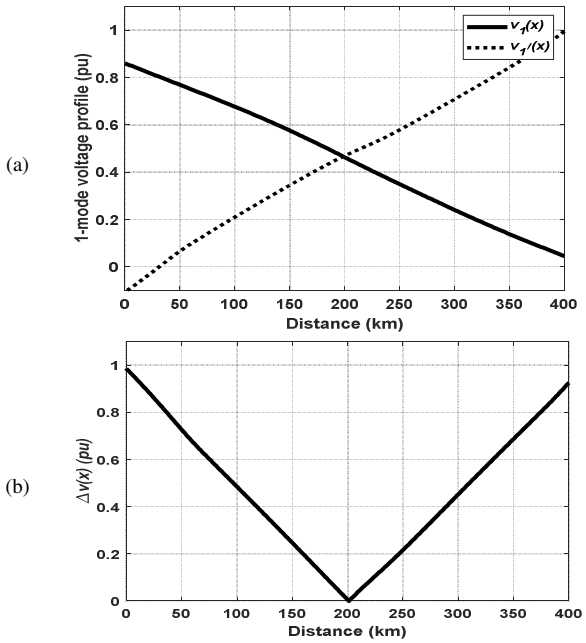

Fig. 5. Obtained results with the fault at the junction point at *F2*. (a) The calculated profile of the 1-mode voltage along the non-homogenous transmission circuit, (b) the profile of the difference among the calculated 1-mode profiles along the adopted non-homogenous circuit.

As shown, the intersection between both profiles occurs at a distance of 200 km, which corresponds to the fault distance. In Figure 5(b), the difference between the calculated profiles of the 1-mode voltages, computed with (4), is illustrated. As shown in Figure 5(b), the minimum value of the difference is found at the distance of 200 km, confirming it as the fault location point. This indicates that loc' equals to 200 km, precisely at the junction point.

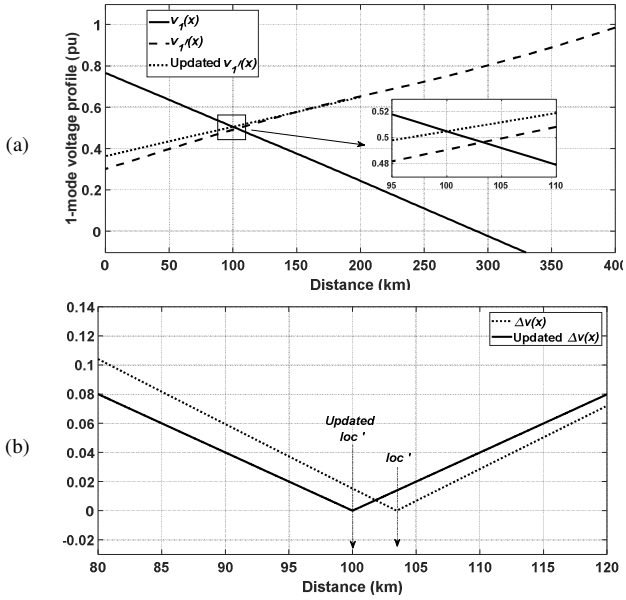

Fig. 6. Obtained results with the fault with the underground cable segment at 100 km from the terminus at *F1*. (a) The calculated profile of 1-mode voltage along the non-homogenous transmission circuit from both ends along with the updated profile along the cable section, (b) the profile of the difference among the calculated 1- mode profiles with and without updating.

B. Fault within the Underground Cable Section

Another fault case is simulated within the underground cable section, specifically 100 km from the transmission line terminus at *F1*. According to the introduced approach, the loc' value is determined first. As seen from the obtained results in Figure 6, the difference between the calculated 1-mode voltage profiles corresponds to a location of 103 km, which is shorter than the cable segment length. Following the introduced approach, this indicates that the fault is within the cable section. Subsequently, the precise fault distance is determined by updating the 1-mode voltage profile along the underground cable section. Figure 6(a) displays the updated $\widetilde{v_1'}(x)$, and Figure 6(b) shows the difference between the 1-mode profiles after the update. It is evident that the minimum value accurately corresponds to the exact location, which is 100 km.

C. Fault within the Overhead Line Section

Another fault case is simulated within the overhead line section, specifically at a location 300 km from the transmission line terminus at *F3*. Following the introduced approach, the value of loc' is first determined.

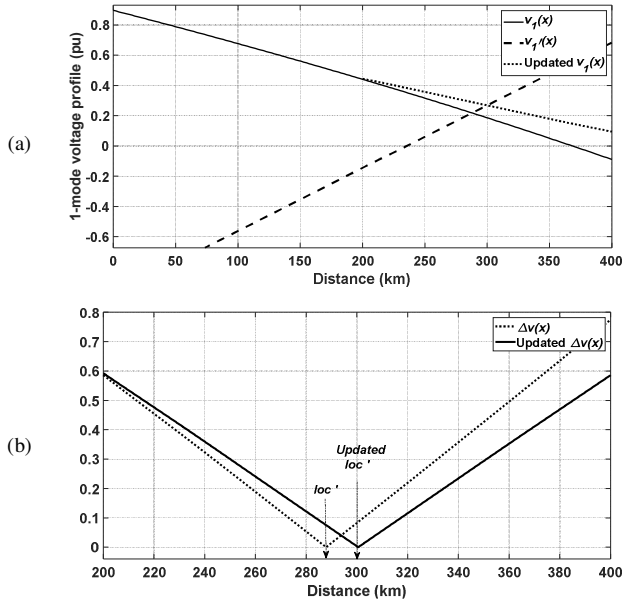

Fig. 7. Obtained results with the fault within the overhead segment at 300 km from the terminus at *F3*. (a) The calculated profile of 1-mode voltage along the non-homogenous transmission circuit from both ends along with the updated profile along the cable section, (b) the profile of the difference among the calculated 1- mode profiles with and without updating.

As demonstrated by the results in Figure 7, the difference between the calculated 1-mode voltage profiles corresponds to a location of 288 km, which exceeds the cable segment length. According to the introduced approach, this signifies that the fault is within the overhead segment. Subsequently, the precise fault distance is determined by updating the 1-mode voltage profile along the overhead line section. Figure 7(a) displays the updated $\widetilde{v_1}(x)$, while Figure 7(b) shows the difference between the 1-mode profiles after the update. It is evident that the minimum value accurately corresponds to the exact location, which is 300 km.

D. Performance under Different Distances with Various Fault Categories

Different fault types, including pole-to-ground and pole-to-pole faults, were tested at diverse fault distances. In each case, the error in the determined fault distance is computed utilizing the following criterion. Table II depicts the obtained results with the tested cases.

$$Error\% = \frac{|\text{Estimated location} - \text{Fault location}|}{\text{Total transmission circuit length}} * 100 \qquad (9)$$

E. Performance under Different Fault Resistances

The introduced fault locator approach is examined under various fault resistance values. Pole-to-pole faults are investigated at three locations: 100, 200, and 300 km, with varying fault resistance values of 10, 50, and 200 **Ω**. Figure 8 illustrates the calculated 1-mode profiles using the introduced approach under various fault resistances.

Figure 8(a) displays the results for the fault at 100 km under three different fault resistance values: 10, 50, and 200 **Ω**. As shown in the results, the intersection point accurately corresponds to the correct fault location, which is 100 km, regardless of the different fault resistance values.

TABLE II. ESTIMATED FAULT LOCATION BY THE INTRODUCED APPROACH UNDER VARIOUS FAULT CATEGORIES AND VARIOUS DISTANCES

Fault type	Fault location (km)	Estimated location (km)	Error %
PG	10	10.3	0.075
PG	60	59.4	0.15
PG	130	128.5	0.375
PG	180	181.1	0.275
PG	210	210.5	0.125
PG	270	268.9	0.275
PG	330	331.2	0.3
PG	390	389	0.25
PP	10	9.8	0.05
PP	60	59	0.25
PP	130	129	0.25
PP	180	180.5	0.125
PP	210	211	0.25
PP	270	271.7	0.425
PP	330	331	0.25
PP	390	392	0.5

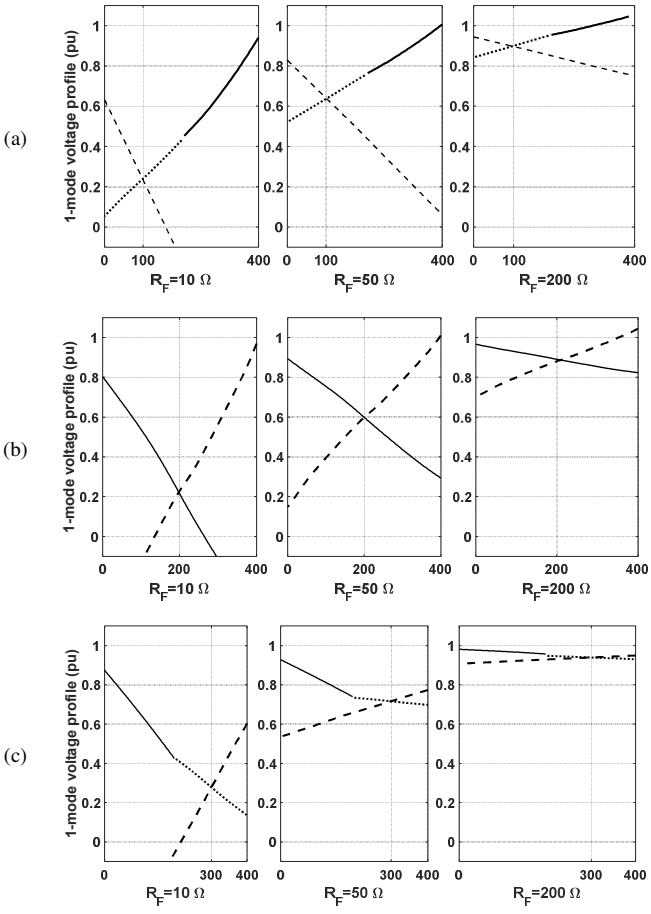

Fig. 8. Obtained results under different fault resistances: Fault at (a) 100 km, (b) 200 km, and (c) 300 km with fault resistances of 10, 50, and 200 **Ω**.

This demonstrates a notable benefit of the proposed method, as it remains unaffected by changes in fault resistance.

Similar results are observed for tests conducted at different locations, as depicted in Figures 8(b)-(c), which show the results for faults occurring at 200 km and 300 km, respectively. It is important to note that the line styles are altered in the Figure to distinguish between the calculated 1-mode voltage profile and the updated profile before and beyond the junction point. In Figures 8(a) and 8(c), solid lines represent the calculated 1-mode voltages, while dashed lines represent the updated voltage profile beyond the junction point. To investigate the error percentage in the obtained locations under different resistances, Table III presents the error percentage calculated according to (9) under the tested cases.

TABLE III. ESTIMATED FAULT LOCATION BY THE INTRODUCED APPROACH UNDER VARIOUS FAULT RESISTANCES

Fault type	Fault distance (km)	Fault resistance (Ω)	Error %
PG	100	5	0.15
PG	100	75	0.09
PG	100	150	0.34
PG	100	250	0.28
PG	200	5	0.25
PG	200	75	0.18
PG	200	150	0.30
PG	200	250	0.21
PG	300	5	0.15
PG	300	75	0.32
PG	300	150	0.27
PG	300	250	0.23
PP	100	5	0.07
PP	100	75	0.11
PP	100	150	0.21
PP	100	250	0.24
PP	200	5	0.18
PP	200	75	0.16
PP	200	150	0.09
PP	200	250	0.31
PP	300	5	0.09
PP	300	75	0.14
PP	300	150	0.31
PP	300	250	0.50

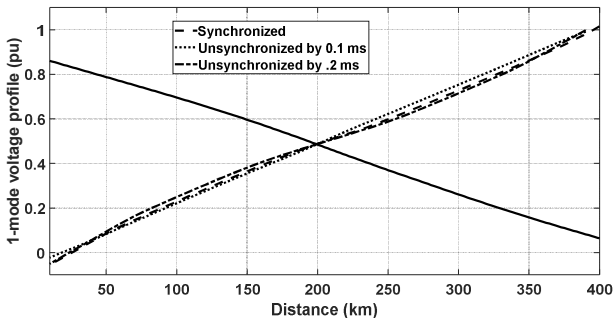

Fig. 9. Obtained results under fault at 200 km with unsynchronized data by 0.1 ms and 0.2 ms.

F. Performance under Unsynchronized Samples at Terminals

The proposed method relies on performing calculations using the recorded signals at the terminals of the transmission circuit. It is essential to test the performance of the introduced approach under unsynchronized samples. Considering the test system mentioned above, a pole-to-pole fault case is simulated at 200 km. The calculations of $\widetilde{v_1}(x)$ are performed with the data recorded at one of the terminals, while the calculations of $\widetilde{v_1}'(x)$ are performed with unsynchronized measured signals.

Figure 9 presents the results of the 1-mode voltage profile under three conditions: synchronized, unsynchronized by 0.1 ms, and unsynchronized by 0.2 ms. As shown in the Figure, the performance is not affected, as the intersection still accurately indicates the fault location, which is 200 km. This demonstrates a significant advantage of the introduced approach.

V. CONCLUSIONS

A fault locator method for non-homogeneous VSC-HVDC transmission circuits is presented in this paper. The method is based on time-domain calculations using signals measured at the terminals. First, the faulted section is identified, either the underground cable or the overhead line. This identification is performed using a proposed criterion based on the comparison of the 1-mode voltage profiles without considering the non-homogeneity of the transmission circuit. Then, the fault locator approach is estimated within the selected section by updating the calculated voltage profile beyond the faulted section. To validate the introduced approach, a non-homogeneous VSC-HVDC transmission system is simulated as a part of integrating an offshore wind farm with the grid. The results confirm the effectiveness of the introduced approach under different fault types, including pole-to-pole and pole-to-ground faults, with a maximum error of 0.5%. Additionally, the approach is tested with changing fault resistance values, even as high as 250 Ω, with errors not exceeding 0.5%. Furthermore, the proposed method is evaluated under synchronization misalignment by 0.1 ms and 0.2 ms, and it is found that its performance remains unaffected. The proposed fault locator is distinguished by its lack of need and for an additional sensor to be installed at the junction point. Furthermore, there is no requirement to visit the site, use extra equipment, or process big data.

ACKNOWLEDGEMENT

The authors gratefully acknowledge the approval and the support of this research study by the grant no. ENGA-2023-12-2311 from the Deanship of Scientific Research at Northern Border University, Arar, Kingdom of Saudi Arabia.

REFERENCES

[1] A. Hameurlaine, H. Sayah, and L. Boukezzi, "Design of Protection Strategies and Performance Analysis of an HVDC Link During Multiple Disturbances," *Engineering, Technology & Applied Science Research*, vol. 12, no. 3, pp. 8760–8764, Jun. 2022, https://doi.org/10.48084/etasr.4992.

[2] P. Ilius, M. Almuhaini, M. Javaid, and M. Abido, "A Machine Learning–Based Approach for Fault Detection in Power Systems," *Engineering, Technology & Applied Science Research*, vol. 13, no. 4, pp. 11216–11221, Aug. 2023, https://doi.org/10.48084/etasr.5995.

[3] K. H. Le and P. H. Vu, "Performance Evaluation of Traveling Wave Fault Locator for a 220kV Hoa Khanh-Thanh My Transmission Line," *Engineering, Technology & Applied Science Research*, vol. 8, no. 4, pp. 3243–3248, Aug. 2018, https://doi.org/10.48084/etasr.2198.

[4] R. S. Narayan, S. Mohan, and K. Sunitha, "Simulative Study into the Development of a Hybrid HVDC System Through a Comparative Research with HVAC: a Futuristic Approach," *Engineering, Technology & Applied Science Research*, vol. 7, no. 3, pp. 1600–1604, Jun. 2017, https://doi.org/10.48084/etasr.1192.

[5] A. Stan, S. Costinaș, and G. Ion, "Overview and Assessment of HVDC Current Applications and Future Trends," *Energies*, vol. 15, no. 3, Jan. 2022, Art. no. 1193, https://doi.org/10.3390/en15031193.

[6] N. Flourentzou, V. G. Agelidis, and G. D. Demetriades, "VSC-Based HVDC Power Transmission Systems: An Overview," *IEEE Transactions on Power Electronics*, vol. 24, no. 3, pp. 592–602, Mar. 2009, https://doi.org/10.1109/TPEL.2008.2008441.

[7] I. E. Davidson, O. E. Oni, A. Aluko, and E. Buraimoh, "Enhancing the Performance of Eskom's Cahora Bassa HVDC Scheme and Harmonic Distortion Minimization of LCC-HVDC Scheme Using the VSC-HVDC Link," *Energies*, vol. 15, no. 11, Jan. 2022, Art. no. 4008, https://doi.org/10.3390/en15114008.

[8] M. Elgeziry, M. Elsadd, N. Elkalashy, T. Kawady, A.-M. Taalab, and M. A. Izzularab, "Non-pilot protection scheme for multi-terminal VSC–HVDC transmission systems," *IET Renewable Power Generation*, vol. 13, no. 16, pp. 3033–3042, 2019, https://doi.org/10.1049/iet-rpg.2018.6265.

[9] M. M. Elgamasy, A.-M. I. Taalab, T. A. Kawady, M. A. Izzularab, and N. I. Elkalashy, "Wave propagation differential protection scheme for VSC-HVDC transmission systems," *Electric Power Systems Research*, vol. 189, Dec. 2020, Art. no. 106826, https://doi.org/10.1016/j.epsr.2020.106826.

[10] M. M. Elgamasy, A.-M. I. Taalab, T. A. Kawady, M. A. Izzularab, and N. I. Elkalashy, "Virtual Difference Voltage Scheme for Fault Detection in VSC-HVDC Transmission Systems," *Journal of Modern Power Systems and Clean Energy*, vol. 8, no. 5, pp. 991–1004, Sep. 2020, https://doi.org/10.35833/MPCE.2019.000172.

[11] A. Xue, J. Zhang, L. Zhang, Y. Sun, J. Cui, and J. Wang, "Transient Frequency Stability Emergency Control for the Power System Interconnected With Offshore Wind Power Through VSC-HVDC," *IEEE Access*, vol. 8, pp. 53133–53140, 2020, https://doi.org/10.1109/ACCESS.2020.2981614.

[12] L. M. Castro and E. Acha, "On the Dynamic Modeling of Marine VSC-HVDC Power Grids Including Offshore Wind Farms," *IEEE Transactions on Sustainable Energy*, vol. 11, no. 4, pp. 2889–2900, Jul. 2020, https://doi.org/10.1109/TSTE.2020.2980970.

[13] H. Rao *et al.*, "The On-site Verification of Key Technologies for Kunbei-Liuzhou-Longmen Hybrid Multi-terminal Ultra HVDC Project," *CSEE Journal of Power and Energy Systems*, vol. 8, no. 5, pp. 1281–1289, Sep. 2022, https://doi.org/10.17775/CSEEJPES.2022.04780.

[14] S. Wu *et al.*, "A Modular Multilevel Converter With Integrated Energy Dissipation Equipment for Offshore Wind VSC-HVDC System," *IEEE Transactions on Sustainable Energy*, vol. 13, no. 1, pp. 353–362, Jan. 2022, https://doi.org/10.1109/TSTE.2021.3111751.

[15] M. M. Elgamasy, M. A. Izzularab, and X.-P. Zhang, "Technical Treating and Riding-Through Symmetrical Grid Faults for MMC-HVDC Connected Offshore Wind Farms," in *23rd International Middle East Power Systems Conference*, Cairo, Egypt, Dec. 2022, pp. 1–6, https://doi.org/10.1109/MEPCON55441.2022.10021810.

[16] O. M. K. K. Nanayakkara, A. D. Rajapakse, and R. Wachal, "Traveling-Wave-Based Line Fault Location in Star-Connected Multiterminal HVDC Systems," *IEEE Transactions on Power Delivery*, vol. 27, no. 4, pp. 2286–2294, Jul. 2012, https://doi.org/10.1109/TPWRD.2012.2202405.

[17] O. M. K. K. Nanayakkara, A. D. Rajapakse, and R. Wachal, "Location of DC Line Faults in Conventional HVDC Systems With Segments of Cables and Overhead Lines Using Terminal Measurements," *IEEE Transactions on Power Delivery*, vol. 27, no. 1, pp. 279–288, Jan. 2012, https://doi.org/10.1109/TPWRD.2011.2174067.

[18] P. Chen, B. Xu, and J. Li, "A Traveling Wave Based Fault Locating System for HVDC Transmission Lines," in *International Conference on Power System Technology*, Chongqing, China, Oct. 2006, pp. 1–4, https://doi.org/10.1109/ICPST.2006.321669.

[19] Q. Huai, L. Qin, K. Liu, H. Ding, X. Liao, and T. Tan, "Combined Line Fault Location Method for MMC–HVDC Transmission Systems," *IEEE Access*, vol. 8, pp. 170794–170806, 2020, https://doi.org/10.1109/ACCESS.2020.3024674.

[20] Y. Ma, H. Li, G. Wang, and J. Wu, "Fault Analysis and Traveling-Wave-Based Protection Scheme for Double-Circuit LCC-HVDC Transmission Lines With Shared Towers," *IEEE Transactions on Power Delivery*, vol. 33, no. 3, pp. 1479–1488, Jun. 2018, https://doi.org/10.1109/TPWRD.2018.2799323.

[21] C. Zhang, G. Song, T. Wang, L. Wu, and L. Yang, "Non-unit Traveling Wave Protection of HVDC Grids Using Levenberg–Marquart Optimal Approximation," *IEEE Transactions on Power Delivery*, vol. 35, no. 5, pp. 2260–2271, Jul. 2020, https://doi.org/10.1109/TPWRD.2020.2964717.

[22] C. Zhang, G. Song, T. Wang, and L. Yang, "Single-Ended Traveling Wave Fault Location Method in DC Transmission Line Based on Wave Front Information," *IEEE Transactions on Power Delivery*, vol. 34, no. 5, pp. 2028–2038, Jul. 2019, https://doi.org/10.1109/TPWRD.2019.2922654.

[23] T. Bi, S. Wang, and K. Jia, "Single pole-to-ground fault location method for MMC-HVDC system using active pulse," *IET Generation, Transmission & Distribution*, vol. 12, no. 2, pp. 272–278, 2018, https://doi.org/10.1049/iet-gtd.2017.0116.

[24] G. Song, T. Wang, and K. S. T. Hussain, "DC Line Fault Identification Based on Pulse Injection From Hybrid HVDC Breaker," *IEEE Transactions on Power Delivery*, vol. 34, no. 1, pp. 271–280, Oct. 2019, https://doi.org/10.1109/TPWRD.2018.2865226.

[25] G.-Y. Kwon *et al.*, "Offline Fault Localization Technique on HVDC Submarine Cable via Time–Frequency Domain Reflectometry," *IEEE Transactions on Power Delivery*, vol. 32, no. 3, pp. 1626–1635, Jun. 2017, https://doi.org/10.1109/TPWRD.2017.2680459.

[26] M. Bawart, M. Marzinotto, and G. Mazzanti, "Diagnosis and location of faults in submarine power cables," *IEEE Electrical Insulation Magazine*, vol. 32, no. 4, pp. 24–37, Jul. 2016, https://doi.org/10.1109/MEI.2016.7528987.

[27] D. Tzelepis, G. Fusiek, A. Dysko, P. Niewczas, C. Booth, and X. Dong, "Novel Fault Location in MTDC Grids With Non-Homogeneous Transmission Lines Utilizing Distributed Current Sensing Technology," *IEEE Transactions on Smart Grid*, vol. 9, no. 5, pp. 5432–5443, Sep. 2018, https://doi.org/10.1109/TSG.2017.2764025.

[28] M. Farshad and J. Sadeh, "A Novel Fault-Location Method for HVDC Transmission Lines Based on Similarity Measure of Voltage Signals," *IEEE Transactions on Power Delivery*, vol. 28, no. 4, pp. 2483–2490, Jul. 2013, https://doi.org/10.1109/TPWRD.2013.2272436.

[29] D. Tzelepis, S. Mirsaeidi, A. Dysko, Q. Hong, J. He, and C. D. Booth, "Intelligent Fault Location in MTDC Networks by Recognizing Patterns in Hybrid Circuit Breaker Currents During Fault Clearance Process," *IEEE Transactions on Industrial Informatics*, vol. 17, no. 5, pp. 3056–3068, Feb. 2021, https://doi.org/10.1109/TII.2020.3003476.

[30] G. Luo, C. Yao, Y. Liu, Y. Tan, J. He, and K. Wang, "Stacked Auto-Encoder Based Fault Location in VSC-HVDC," *IEEE Access*, vol. 6, pp. 33216–33224, 2018, https://doi.org/10.1109/ACCESS.2018.2848841.

[31] G. Song, X. Chu, X. Cai, S. Gao, and M. Ran, "A fault-location method for VSC-HVDC transmission lines based on natural frequency of current," *International Journal of Electrical Power & Energy Systems*, vol. 63, pp. 347–352, Dec. 2014, https://doi.org/10.1016/j.ijepes.2014.05.069.

[32] J. Suonan, S. Gao, G. Song, Z. Jiao, and X. Kang, "A Novel Fault-Location Method for HVDC Transmission Lines," *IEEE Transactions on Power Delivery*, vol. 25, no. 2, pp. 1203–1209, Apr. 2010, https://doi.org/10.1109/TPWRD.2009.2033078.

[33] L. Yuansheng, W. Gang, and L. Haifeng, "Time-Domain Fault-Location Method on HVDC Transmission Lines Under Unsynchronized Two-End Measurement and Uncertain Line Parameters," *IEEE Transactions on Power Delivery*, vol. 30, no. 3, pp. 1031–1038, Jun. 2015, https://doi.org/10.1109/TPWRD.2014.2335748.

[34] M. M. Elgamasy, M. A. Izzularab, and X.-P. Zhang, "Single-End Based Fault Location Method for VSC-HVDC Transmission Systems," *IEEE Access*, vol. 10, pp. 43129–43142, 2022, https://doi.org/10.1109/ACCESS.2022.3169777.

[35] J. Xu, Y. Lu, C. Zhao, and J. Liang, "A Model-Based DC Fault Location Scheme for Multi-Terminal MMC-HVDC Systems Using a Simplified Transmission Line Representation," *IEEE Transactions on Power Delivery*, vol. 35, no. 1, pp. 386–395, Oct. 2020, https://doi.org/10.1109/TPWRD.2019.2932989.